Broadband Coaxial S-Parameter Measurements for Cryogenic Quantum Technologies

Sang-Hee Shin, *Member, IEEE*, Manoj Stanley, *Member, IEEE*, James Skinner, *Member, IEEE*, Sebastian E. de Graaf, and Nick M. Ridler, *Fellow, IEEE*

***Abstract*— Development of RF and microwave metrology capabilities at cryogenic temperatures is critical for the development of high-performance microwave devices to facilitate commercialization of cryogenic quantum technologies. This article presents a broadband microwave S-parameter calibration scheme suitable for cryogenic environments operating at temperatures down to tens of milli-kelvin (mK). The technique is based on a weighted multi-line thru-reflect-line (TRL) calibration approach and is demonstrated using coaxial air line calibration standards. One- and two-port microwave devices commonly used in cryogenic quantum computing applications, a cryogenic 50 Ω matched load and a cryogenic 6 dB attenuator, were measured. The measured results at mK temperatures indicate that when combined with calibration standards of appropriate electrical length, the weighted multi-line TRL calibration scheme allows broadband frequency coverage compared to conventional TRL calibration schemes utilizing a single line standard. The mechanical and electrical properties of the line standards at mK temperatures were investigated and discussed. These findings establish the feasibility of utilizing multiple off-the-shelf coaxial air lines to enhance the frequency range of calibrations at mK temperatures.**

***Index Terms*— Low temperature measurement, microwave calibration, S-parameters, superconducting quantum, thru-reflect-line (TRL) calibration.**

I. Introduction

CRYOGENIC quantum technologies such as quantum computing and quantum sensing utilize RF and microwave components operating at temperatures down to tens of milli-kelvin (mK) [1], [2]. Microwave components commonly used at mK temperatures for these applications are attenuators, circulators, isolators, etc. [2], [3]. Typically, these components are not designed for operation in cryogenic environments (<−200 °C) and manufacturers typically characterize the devices only over a limited temperature range (−40 °C to +80 °C). Due to potential changes in material properties such as the dielectric constant of substrate materials, resistivity of metal conductors, and thermal contraction at cryogenic temperatures, S-parameters of devices are likely to change when operating in such conditions. For example, attenuators and matched loads feature resistors that are potentially temperature dependent [4]. Therefore, the components need to be characterized at the operating temperature to ensure reliable operation.

To characterize these components precisely, implementing appropriate calibration routines is essential. This is particularly important in the cryogenic environment as lossy cables, interconnects, and attenuators are used to connect the devices under test (DUTs) inside a dilution refrigerator with test instruments such as the vector network analyzer (VNA) operating at room temperature. Implementing an appropriate calibration scheme allows the calibration reference plane to be placed as close to the DUT as possible.

Several VNA-based calibration methods have been proposed to characterize a DUT at cryogenic temperatures. For example, in [5], silicon-based on-chip calibration standards were used to implement a conventional thru-reflect-line (TRL) two-port calibration. However, the technique was only applicable over a limited frequency range of up to 4.5 GHz. In [6], a two-port calibration technique using a TRL scheme was implemented at 6.6 K for measuring superconducting microwave resonators.

In [7], a single-port calibration technique using short-open-load (SOL) standards was implemented at 4.2 K using polymer-based conductor-backed co-planar waveguide (CPW) calibration standards.

Stanley et al. [8], [9] have recently demonstrated PCB-based calibration standards suitable for use in the cryogenic environment.

S-parameter calibrations for coaxial-based device measurements have been demonstrated at mK temperatures using dielectric-filled coaxial standards [10], [11]. However, in the cryogenic environment, the characteristics of polymer-based dielectrics are very difficult to precisely predict, and this will compromise the accuracy and reliability of the calibration.

This study focuses on using coaxial air lines as calibration standards. Air lines are coaxial transmission lines that feature air as the dielectric rather than polytetrafluoroethylene (PTFE) or some other material. As a result, air lines have highly predictable characteristics with very low reflection and transmission loss that can be modeled using the mechanical dimensions of air line. This makes them ideal for the cryogenic environment as they avoid uncertainties associated with dielectric-filled coaxial standards. Recently, Stanley et al. [12]

Manuscript received 22 June 2023; revised 25 August 2023; accepted 1 October 2023. Date of publication 17 October 2023; date of current version 4 April 2024. This work was supported by the U.K. Government's Department for Science, Innovation and Technology (DSIT) through the U.K. National Quantum Technologies Program. *(Corresponding author: Sang-Hee Shin.)*

The authors are with the National Physical Laboratory, TW11 0LW Teddington, U.K. (e-mail: ssh1625@gmail.com; manoj.stanley@npl.co.uk; james.skinner@npl.co.uk; sebastian.de.graaf@npl.co.uk; nick.ridler@npl.co.uk).

Color versions of one or more figures in this article are available at https://doi.org/10.1109/TMTT.2023.3322909.

Digital Object Identifier 10.1109/TMTT.2023.3322909

and Skinner et al. [13] have demonstrated the feasibility of using custom-made air lines as calibration standards using the TRL calibration scheme incorporating a single line standard. In this article, an improved, broadband (up to 18 GHz) calibration technique utilizing weighted multi-line TRL is demonstrated for characterizing S-parameters of two-port devices at mK temperatures. Commercially available long air line calibration standards with electrical lengths of multiples of the operating wavelengths are used to characterize the devices. The DUTs include a cryogenic attenuator and a cryogenic 50 Ω near-matched load. The electrical properties of the air lines at mK temperatures such as electrical length, resistivity, and characteristic impedance are also determined and compared with room temperature determinations. The feasibility of utilizing multiple long air line calibration standards at mK temperatures is assessed and the sources of measurement error are discussed.

II. Measurement Setup

This section describes the measurement setup used to perform the S-parameter measurements of the DUTs at both room temperature (taken here to be 296 K) and mK temperatures. A two-port Keysight PNA N5222B VNA was used for the S-parameter measurements at both temperatures. It is impractical to measure each of the calibration standards and DUTs over separate cooling cycles due to the long cooling period of 2–3 days required to operate a dilution refrigerator operating at mK temperatures. Moreover, connecting and disconnecting the calibration standards and DUTs between cooldowns will introduce additional errors. For rapid measurements, we remotely switch between each calibration standard and DUT using a pair of six-port cryogenic RF switches [Radiall SP6T Ramses subminiature version A (SMA)] [8], [9], [10], [11], [12], [13]. This approach also minimizes calibration and measurement errors due to system drift and other random error sources such as noise. Each standard is connected to the switches using phased-matched, semi-rigid cryogenic coaxial cables manufactured by Maury Microwave. The two RF switches (dc to 18 GHz) used in the calibration unit are commercially available mechanical pulse-latched SP6T switches. The switches operate by means of electrical pulses (28 V_{pp} at 296 K and 5 V_{pp} at 30 mK) of short duration (10 ms) to latch the switch to different positions, so no electrical signal is applied to the switch in its quiescent state. The switches are software controlled to activate/deactivate the respective standard/DUT during the measurements. A switching pulse results in an increase in cryostat temperature of only a few mK for a brief period. Therefore, a significant waiting period is not required to perform the full calibration at mK temperatures, minimizing drift errors. The pre-connected switch setup is shown in Fig. 1. Each switch is populated with five 3.5 mm TRL calibration standards and one DUT. The switches are mounted on copper fixtures to thermalize the setup. With five calibration standards, only one pair of switch ports is available for the DUT. Therefore, two measurement cycles were undertaken to measure the two DUTs (the 6 dB attenuator and the 50 Ω matched load). The frequency range was limited to 18 GHz as this is the upper limit of the SMA cables utilized inside the dilution refrigerator.

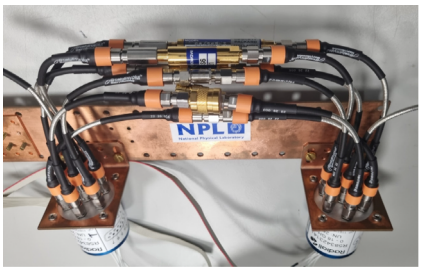

Fig. 1. Photograph of the calibration unit showing a pair of SP6T switches populated with five calibration standards and a DUT.

TABLE I
Properties of Measured Devices

DUTs	Connector type	Manufacturer	Nominal Operating Frequency range
6 dB attenuator	SMA	APItech	< 18 GHz
Matched load (Nominal Impedance: 50 Ω)		Quantum Microwave	4 – 12 GHz

Uncalibrated S-parameter measurements of the calibration standards and DUTs were recorded for offline post-calibration. The calibration standards are described in Section III. Table I summarizes the DUTs measured in this study.

A. Room Temperature Measurement

For the room temperature (taken here to be 296 K) setup, each port of the VNA is connected to the common port of each of the switches using a pair of metrology grade, phase-stable 3.5 mm coaxial cables and semi-rigid coaxial cables. The schematic illustration and in situ measurement setup are shown in Fig. 2(a) and (b), respectively.

B. mK Measurement

For the mK S-parameter measurements, the switch system was mounted inside the dilution fridge's mixing chamber (<30 mK during the measurement). The dilution refrigerator has six different temperature stages: room temperature (296 K), 50 K, 4 K, 800 mK, 100 mK, and ∼30 mK. The cryogenic measurement setups used in [8] to characterize quantum circuits typically consisted of coaxial lines of high attenuation (i.e., of 60 dB or more) which reduce the population of microwave photons to ensure reliable operation of the quantum devices and minimize heating inside the dilution refrigerator. However, this approach requires multiple amplification stages to generate acceptable signal levels for the VNA measurements. These architectures present difficulties in terms of VNA receiver linearity [14] and for measuring the VNA switch terms, which are used to account for the change in reflection coefficient of the VNA's internal switch ports.

Therefore, to enable characterization of the standards in this environment, we have utilized a measurement architecture with minimum attenuation when characterizing a microwave device, thus eliminating the need for amplification stages, as shown in Fig. 3(a).

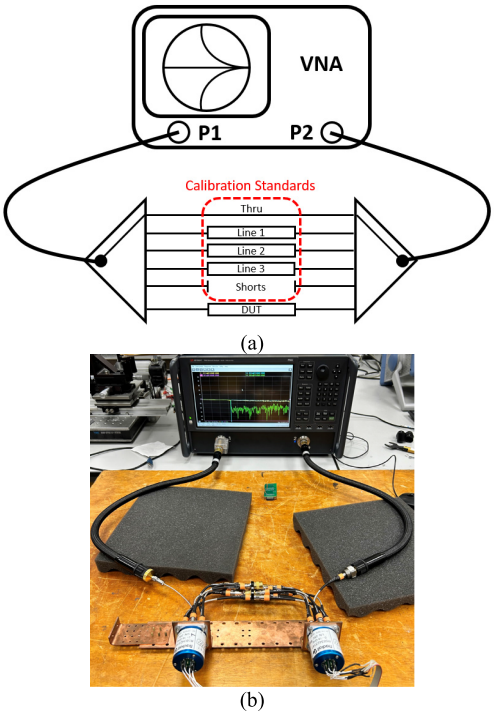

Fig. 2. Room temperature measurement setup. (a) Schematic illustration. (b) In situ measurement setup.

This is similar to the measurement architectures used in [12] and [13] for characterizing microwave devices at mK temperatures. Long lossy cables and a series of fixed attenuators are included on each of the coaxial paths inside the cryostat to limit the RF signal power entering the mixing chamber [15]. The insertion loss between the DUTs and the VNA test ports is estimated to be around 10 dB at 0.5 GHz, increasing to around 25 dB at 18 GHz. The output power from the VNA is -10 dBm. Therefore, the signal power at DUT input is less than -20 dBm (10 μW). This signal power is lower than the cooling power (15 μW) of the mK stage in the dilution refrigerator. Therefore, there was no observable temperature increase at the base. The switch set-up featuring the calibration standards and DUTs was directly attached to the baseplate using a copper plate for thermalization. Note that the power dissipated in the DUTs may go under these conditions up to a few μW, meaning the DUT may be at a temperature slightly above that of the refrigerator. Reducing the power at the DUT by reducing the VNA output power or by increasing the attenuation in the higher temperature stages would improve this at the expense of increased calibration errors due to lower signal levels. Attenuators are installed at the 50 K stage to reduce thermal radiation and increase the thermal stability of the cables. Fig. 3(b) shows the switch system mounted inside the dilution refrigerator.

Finally, the VNA IF bandwidth was set to 10 Hz, with no averaging. Although averaging can potentially help reduce random errors such as noise, when using the mK RF measurement system, longer sweep time risks an increase in drift errors. Therefore, averaging was not applied in order to limit the sweep time.

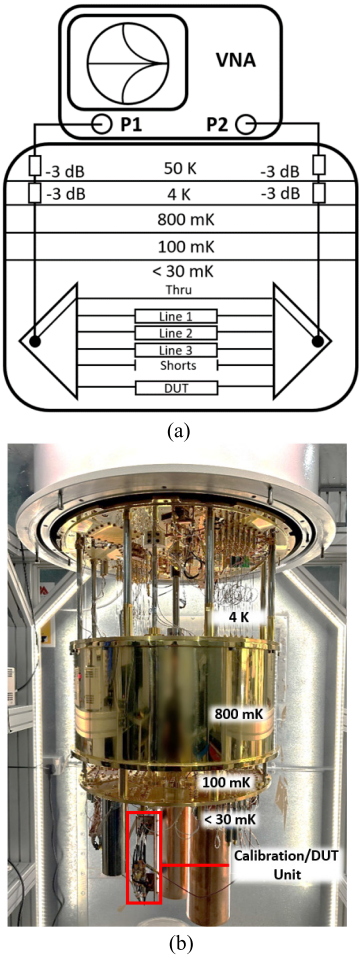

Fig. 3. mK measurement setup situated inside the dilution refrigerator. (a) Schematic illustration. (b) Photograph.

III. Calibration

Effective calibration of a VNA is critical for accurate S-parameter measurements. Conventionally, for two-port room temperature measurements, calibration schemes such as short-open-load-thru (SOLT) [16], thru-reflect-match (TRM) [17], and TRL [18] are used. SOLT and TRM are routinely used for room temperature coaxial measurements as they do not require air lines which can be expensive and difficult to use. However, these schemes require one or more of the calibration standards to be accurately pre-defined [19] at the operating temperature. This may not be possible at mK temperatures as the performance of standards, such as matched loads, may change when cooled down. With the TRL scheme, the calibration standards do not need to be accurately defined prior to the calibration, only requiring the reflect standards used for each port to be identical. This makes the TRL calibration well suited for the cryogenic environment.

Despite these advantages, the conventional 1/4-wave TRL calibration scheme is not without drawbacks. First, TRL is band limited. The conventional TRL calibration scheme utilizes a transmission line of quarter-wave delay as the line standard. At frequency ranges where the relative phase of the line standard approaches 0° or 180°, the calibration fails due to phase ambiguity. Typically, the TRL calibration is considered

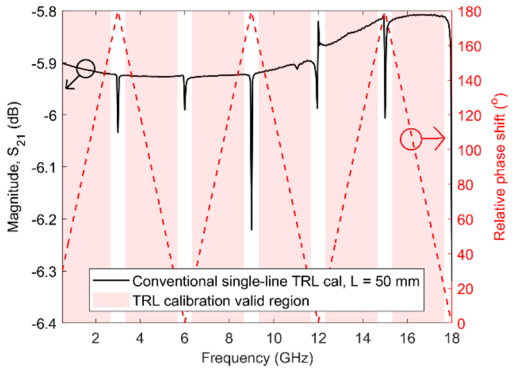

Fig. 4. Example of TRL calibration failure points.

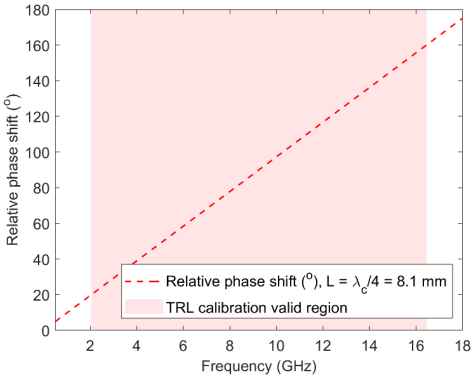

Fig. 5. Calculated relative phase shift for the 1/4-wave line standard.

reliable for frequency ranges where the line standard's relative phase is between 20° and 160° [20].

Using an inappropriate line standard can result in multiple calibration failures across the frequency band. Fig. 4 shows an example of calibration failures due to use of an inadequate line standard. The shaded regions show where the performance of calibration is acceptable, i.e., where the line standard's relative phase is between 20° and 160°, with the failure points indicated by the spikes in the black trace.

For conventional single-line TRL, using a quarter-wave line at the center of the frequency band will provide the most extensive coverage of the frequency range. However, as shown in Fig. 5, a single quarter-wave line of length 8.1 mm is insufficient to cover the entire frequency range of interest in this work (0.5–18 GHz). Use of this line will result in calibration failure will near the band edges, specifically below 2 GHz and above 16.2 GHz. In addition, it is impractical to construct a 3.5 mm coaxial air line with a mechanical length of less than 9 mm without necessitating a specialized adapter to mount the short air line.

To address the above issues, in this study, we opted for an approach where three line standards with different lengths were utilized. Each line was selected to cover specific frequency ranges, and by combining the results from these three line standards in an appropriate manner, the performance of the calibration would be acceptable over the entire frequency band.

Three commercially available 3.5 mm air lines of different lengths were selected: 50, 60, and 75 mm. The relative phase

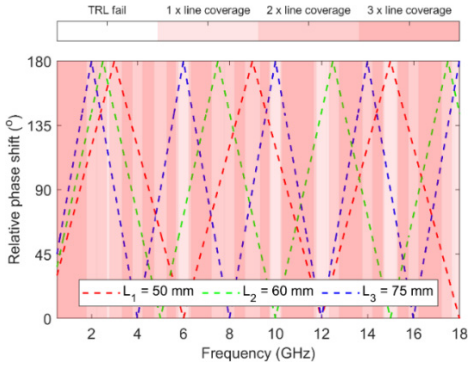

Fig. 6. Calculated relative phase shift for the line standards.

shifts of each air line were calculated and are presented in Fig. 6. The shaded regions represent the phase coverage ranging from 20° to 160° for each line. Notably, the entire plot area is shaded, indicating that every frequency across the range is covered. The darker shaded areas indicate that the corresponding frequency ranges are covered more than once, ensuring robust coverage across the entire frequency band.

With three line standards selected to sufficiently cover the entire frequency band, the next step is to determine an appropriate method of combining the results from the individual line standards. Frequency ranges can be assigned to each line standard and results from each combined without any overlapping frequencies. This is a viable approach for use of a conventional 1/4-wave TRL calibration kit, which typically involves only a few transitions over the frequency range of interest. With our three-line setup this is not practical, as the relatively long lengths of the lines give rapidly changing relative phase and so would involve over 20 transitions across the frequency range. In addition, this method can cause artifacts such as discontinuities due to abrupt changes in the results from one line to another [21]. To avoid these problems, a systematic combining scheme is introduced in a post-processing step that effectively combines the results from all three line standards. The discontinuities will be removed by using the proposed combining scheme.

At each frequency point, the results are weighted according to the confidence in the calibration. For example, the scheme assigns weights of a line to be 1 and 0 when the relative phases are 90° and 0°, respectively. The weights (w_i) are determined according to the following:

$$w_i = \sin^n \varphi_i \tag{1}$$

where φ_i is calculated relative phase shift of the ith line standard and n is a power coefficient that determines the shape of the weighting curve. The coefficient n needs to be an even integer as the weight cannot be a negative value. Fig. 7 shows the calculated weights for the 50 mm air line standard. As shown in Fig. 7, $n = 4$ was chosen as it rejects the TRL calibration failure region ($\varphi_i \approx 180°$) more effectively than $n = 2$. Note that alternative functions for determining weights could be employed to enhance the calibration accuracy. However, a detailed exploration of these

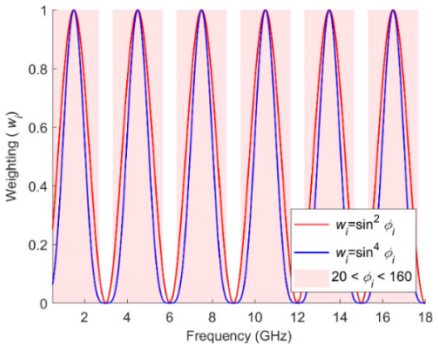

Fig. 7. Calculated weights for the 50 mm air line.

TABLE II
SPECIFICATIONS OF THE CALIBRATION STANDARDS

Calibration Standards	Manufacturer	Connector type	Nominal Lengths (mm)
Thru	N/A	3.5 mm	0
Line 1	Maury Microwave		50
Line 2			60
Line 3			75
Offset Shorts			N/A

functions and their impact on calibration accuracy falls beyond the scope of this article.

The final S-parameter result, S_f (real and imaginary), is determined using the weighted mean of the S-parameter data

$$S_f = \frac{\sum_{i=1}^{3} w_i S_i}{\sum_{i=1}^{3} w_i} \tag{2}$$

where S_i is the TRL-corrected S-parameter data using the line standard, i. Further investigation will be required to quantify the uncertainty for this type of cryogenic S-parameter measurement.

A. Calibration Standards

The female and male connectors of each port at the calibration reference plane were connected to establish a zero-length "Thru" connection, ensuring zero phase delay. With the Thru connection, forward and reverse switch correction terms were measured as well as the standard two-port uncalibrated S-parameters [22]. For the Reflect standards, 3.5 mm male and female coaxial offset short circuits were selected, both with an offset length of 5.1 mm. The three aforementioned air lines utilized as the line standards were manufactured by Maury Microwave. Table II summarizes the specifications of the calibration standards.

IV. Measurement Results and Discussion

A. 6 dB Attenuator

Fig. 8(a)–(c) shows calibrated S_{21} magnitude, S_{21} phase, and S_{11} magnitude of the 6 dB attenuator, respectively, at room and mK temperatures. Results of measurements taken at room temperature without using the switch system are included as a reference. This reference measurement will not suffer from any error contributions relating to the RF coaxial switches or cables connecting the switches to the standards and DUT.

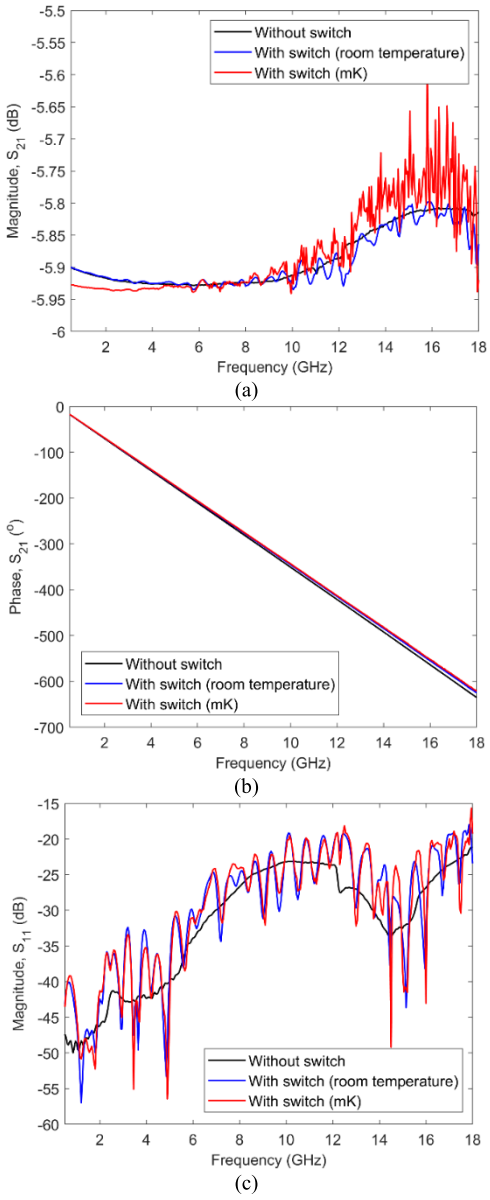

Fig. 8. Calibrated S-parameter results for the cryogenic 6 dB attenuator. (a) Magnitude of S_{21}. (b) Phase of S_{21}. (c) Magnitude of S_{11}.

The room temperature and mK measurements show good agreement for both the S_{21} and S_{11} results. Fig. 8(a) shows that at the lower frequencies (<10 GHz), the deviation between the room temperature and the mK results is less than 0.03 dB. However, at the higher frequencies (>10 GHz), it can be seen that the mK measurement results have more noisy ripples compared to the room temperature results. This could be due to higher path losses at higher frequencies induced by the long coaxial cables and coaxial interconnects inside the cryostat that are installed between the VNA and the switch system.

From Fig. 8(b), it is evident that there are slight transmission phase differences between the room temperature and mK results. The measured transmission phases of the 6 dB attenuator at mK temperature were consistently smaller across

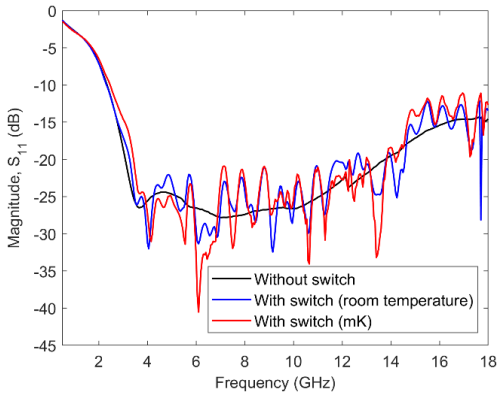

Fig. 9. Calibrated S_{11} of the cryogenic 50 Ω matched load.

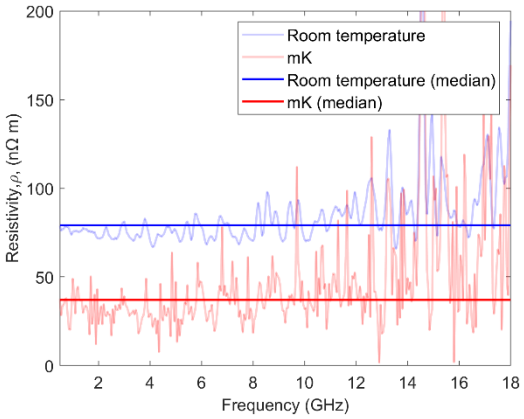

Fig. 10. Calculated resistivity of the 50 mm air line at room temperature and mK temperatures.

all frequencies, and this difference becomes more pronounced as the frequency increases. At 18 GHz, a maximum deviation of 3.5° was observed.

For the S_{11} results, there is no significant deviation between the room temperature and the mK measurements across the whole frequency range as shown in Fig. 8(c).

Fig. 8 also shows additional ripples in the results with switches when compared to the results without switches. This is mainly due to variations in transmission length and loss between the different RF switch port paths and the coaxial cables connected to each of these switch ports. Other factors such as differences in source match of switch ports and repeatability of switch port performance could also have an impact.

B. Matched Load

Fig. 9 shows calibrated S_{11} results of the cryogenic matched load at room temperature and mK temperatures. Note that the operational frequency range of the matched load specified by the manufacturer is 4–12 GHz. There are only minor differences between the room temperature and mK results. The degradation in performance below 4 GHz can also be observed in the results at both temperatures, which is expected to be due to this being outside the designed operating frequency range of the load. Within the manufacturer specified operational frequency range (4–12 GHz), the cryogenic matched load performs very well, as shown by the S_{11} results less than −20 dB throughout the specified frequency range at both room temperature and mK temperatures.

C. Air Line Characteristics

In this section, the resistivities, characteristic impedances, and electrical lengths of the air line standards are derived from their observed loss.

The characteristic impedance (Z) of a transmission line is defined as

$$Z = \sqrt{\frac{R + j\omega L}{G + j\omega C}} \tag{3}$$

where ω is the angular frequency and the circuit elements R, L, G, and C are series resistance, series inductance, shunt conductance, and shunt capacitance, respectively. To calculate these circuit elements, first the air line is assumed to be lossless where the series resistance and shunt conductance are considered to be zero. The lossless series inductance and shunt capacitance of the air line can be calculated using expressions from [23] and [24]. The values for the radii of the inner (a) and outer (b) conductors at room temperature are required for the calculation. Mechanically measured values are obtained using the air-gauging method [25]. For a change in temperature from 296 K to mK temperatures, the dimensions of the air lines are estimated to contract by 0.3% by first order approximation due to thermal contraction of the conductor metal (beryllium copper—BeCu) [26]. However, as the air lines have small losses due to the finite conductivity of the conductor elements, certain corrections to account for these losses need to be applied [23]. To calculate the equivalent circuit elements of a lossy air line, the attenuation constant (α) is extracted from the S-parameter measurements using the following equation:

$$\alpha = \frac{-\ln\left|\frac{|S_{21}|+|S_{12}|}{2}\right|}{l} \tag{4}$$

where l is the length of the air line. From the extracted α and dimensions of the air line conductors, the high-frequency resistivity (ρ) is approximated using the following equation from [23]:

$$\rho = \left[\frac{200\alpha b}{1 + \frac{b}{a}}\right]^2 \frac{\pi}{\mu_0 f} \tag{5}$$

where μ_0 is the free-space permeability ($4\pi \times 10^{-7}$ H/m) and f is the frequency. The calculated resistivity of the 50 mm air line is shown in Fig. 10. The equivalent circuit elements (R, L, G, and C) are then calculated taking into account the calculated resistivity.

As expected, Fig. 10 clearly shows that the resistivity of the air line is reduced at mK temperatures. There is no clear frequency dependence in the calculated resistivity, therefore it is considered appropriate to summarize the resistivity using an average (i.e., the median) value. At room temperature, the median value of resistivity for the 50 mm air line is 79 nΩ·m; at mK temperature, it is 37 nΩ·m. The calculated resistivity

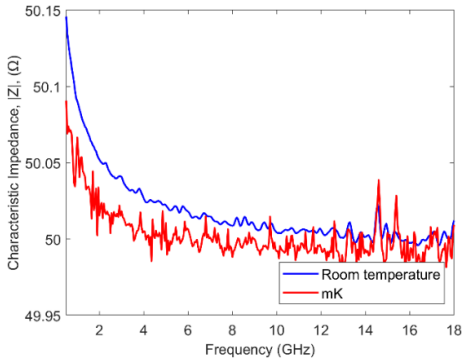

Fig. 11. Extracted characteristic impedance magnitude of the 50 mm air line at room temperature and mK temperatures.

of the 50 mm air line has reduced by approximately 50%. The air line has inner and outer conductors made of BeCu and plated with a thin gold layer. The plating thickness is unknown. According to [26], the resistivity of BeCu at 4 K is 20%–40% lower than at room temperature, although this is also dependent on the composition and thermal treatments. Furthermore, the resistivity of gold is reported to reduce significantly (>90%) at 4 K [27]. As a result, our estimate of ≈50% reduction in air line resistivity at the mK temperatures can be considered reasonable. These results indicate that even though the conductor material of the air line is not expected to be superconducting over the mK temperature range of our experiment (30 mK), the reduction in resistivity is significant and may impact the characteristic impedance.

The characteristic impedance of air lines is calculated using (3), incorporating the losses in the air line. The characteristic impedance of the 50 mm air line is shown in Fig. 11.

According to the results in Fig. 11, there are small but noticeable differences in the characteristic impedance across the frequency range. Despite a significant reduction in resistivity, the extracted characteristic impedances at mK were typically only around 0.03% smaller compared to the room temperature determinations. These findings suggest that these air lines can still function as reliable impedance references for TRL calibration at mK temperatures.

Finally, the electrical lengths of the air line standards are extracted from transmission phase measurements to observe any thermal contraction. The extracted lengths are then corrected to reflect the measured electrical losses using the method shown in [23]. The extracted electrical lengths for lossless (uncorrected) and lossy (corrected) air lines at room temperature and mK temperatures are shown in Fig. 12.

The results in Fig. 12 indicate that at mK temperatures the air lines have shorter electrical lengths than at room temperature due to thermal contraction. The electrical lengths of the 50, 60, and 75 mm air lines are reduced by 0.30%, 0.37%, and 0.37%, respectively. Analytical thermal contraction (ΔL) of the air lines due to change in temperature (ΔT = 296 K–30 mK) can be predicted using

$$\Delta L = c_{\text{te}} L_0 \Delta T \tag{6}$$

where c_{te} is the coefficient of thermal expansion and L_0 is the length of the air line at room temperature. The coefficient

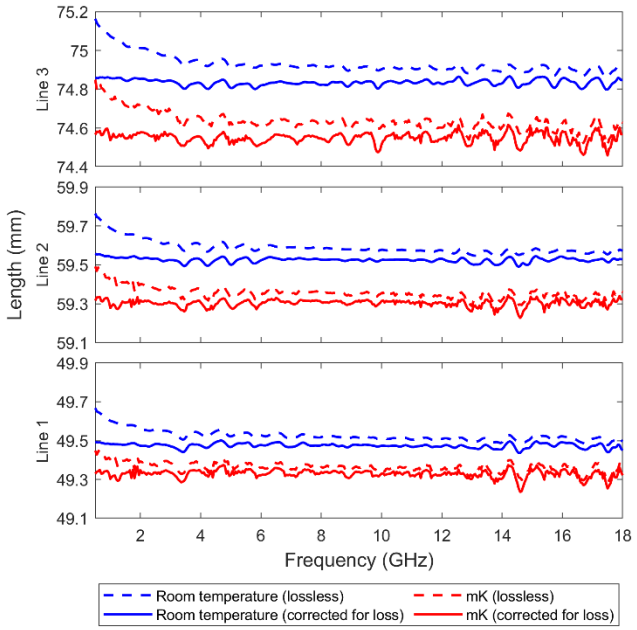

Fig. 12. Extracted air line lengths (uncorrected and corrected for the air line loss) at room temperature and mK.

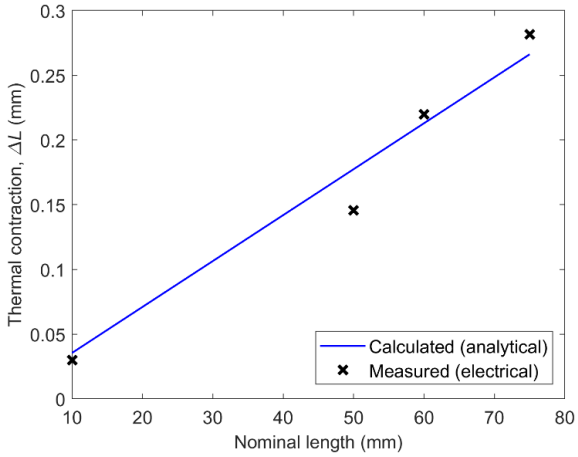

Fig. 13. Analytically predicted and extracted thermal contractions of air lines operating at mK temperatures.

of thermal expansion was extrapolated from [26]. Fig. 13 shows the comparison of analytical prediction and extracted thermal contraction of the air lines. In addition, data from a 10 mm air line from the authors' previous work [13] has been included for comparison. The analytically predicted and measured (extracted) values demonstrate strong agreement, indicating the reliability of this analysis. Moreover, the results validate our previous assumption of a 0.3% reduction in air line dimensions for estimating resistivity.

It is important to note that the difference in electrical length and loss in the switch paths and the cables have an observable impact on the measured and calculated results [12]. To minimize these errors, phase-matched cables and cryogenic switches were used in this study.

V. Conclusion

This study demonstrated a broadband microwave calibration scheme for S-parameter measurement at cryogenic (30 mK) temperatures. A weighted multi-line TRL calibration scheme

using a set of three 3.5 mm coaxial air line calibration standards was employed to measure one- and two-port cryogenic devices typically used in quantum computing applications. The measured results have shown that with appropriate selection of line standards, the weighted multi-line TRL calibration scheme offers effective broadband coverage at mK temperatures that is otherwise challenging to achieve with the conventional single-line TRL approach. Despite the significant reduction in resistivity of the air line materials at low temperatures, only a minimal change in characteristic impedance was observed (0.03%). Furthermore, the extracted thermal contraction of the line standards shows that the thermal contraction behaviors were highly predictable even using only first-order approximations. In conclusion, the study highlights that the employed measurement technique, utilizing multiple air line standards, is an effective calibration approach for characterizing microwave components at cryogenic temperatures over a broad frequency range for applications in cryogenic quantum technologies.

ACKNOWLEDGMENT

The authors would like to thank Dr. Jonas Urbonas of Maury Microwave Corporation, Ontario, CA, USA, for supporting this work.

REFERENCES

[1] J. C. Bardin, D. H. Slichter, and D. J. Reilly, "Microwaves in quantum computing," *IEEE J. Microw.*, vol. 1, no. 1, pp. 403–427, Jan. 2021.

[2] P. Krantz, M. Kjaergaard, F. Yan, T. P. Orlando, S. Gustavsson, and W. D. Oliver, "A quantum engineer's guide to superconducting qubits," *Appl. Phys. Rev.*, vol. 6, no. 2, Jun. 2019, Art. no. 021318.

[3] A. Cridland, J. Lacy, J. Pinder, and J. Verdú, "Single microwave photon detection with a trapped electron," *Photonics*, vol. 3, no. 4, p. 59, Nov. 2016.

[4] N. D. Orloff et al., "A compact variable-temperature broadband series-resistor calibration," *IEEE Trans. Microw. Theory Techn.*, vol. 59, no. 1, pp. 188–195, Jan. 2011.

[5] D. E. Oates, R. L. Slattery, and D. J. Hover, "Cryogenic test fixture for two-port calibration at 4.2 K and above," in *Proc. 89th ARFTG Microw. Meas. Conf.*, Honolulu, HI, USA, 2017, pp. 1–4.

[6] J.-H. Yeh and S. M. Anlage, "In situ broadband cryogenic calibration for two-port superconducting microwave resonators," *Rev. Sci. Instrum.*, vol. 84, no. 3, Mar. 2013, Art. no. 034706.

[7] P. Diener et al., "Cryogenic calibration setup for broadband complex impedance measurements," in *Proc. 15th Int. Conf. Transp. Interacting Disordered Syst.*, Sant Feliu de Guixols, Spain, 2013, pp. 1–5.

[8] M. Stanley, S. De Graaf, T. Hönigl-Decrinis, T. Lindström, and N. M. Ridler, "Characterizing scattering parameters of superconducting quantum integrated circuits at milli-Kelvin temperatures," *IEEE Access*, vol. 10, pp. 43376–43386, 2022.

[9] M. Stanley, R. Parker-Jervis, S. de Graaf, T. Lindström, J. E. Cunningham, and N. M. Ridler, "Validating S-parameter measurements of RF integrated circuits at milli-Kelvin temperatures," *Electron. Lett.*, vol. 58, no. 16, pp. 614–616, Jun. 2022.

[10] S. Simbierowicz, V. Y. Monarkha, S. Singh, N. Messaoudi, P. Krantz, and R. E. Lake, "Microwave calibration of qubit drive line components at millikelvin temperatures," *Appl. Phys. Lett.*, vol. 120, no. 5, Jan. 2022, Art. no. 054004.

[11] L. Ranzani, L. Spietz, Z. Popovic, and J. Aumentado, "Two-port microwave calibration at millikelvin temperatures," *Rev. Sci. Instrum.*, vol. 84, no. 3, Mar. 2013, Art. no. 034704.

[12] M. Stanley, S.-H. Shin, J. Skinner, J. Urbonas, and N. Ridler, "Characterising scattering parameters of coaxial microwave devices at milli-Kelvin temperatures for quantum computing technologies," in *Proc. Eur. Microw. Conf. (EuMC)*, Berlin, Germany, 2023, pp. 150–153.

[13] J. Skinner, M. Stanley, J. Urbonas, S. de Graaf, T. Lindström, and N. Ridler, "Characterizing precision coaxial air lines as reference standards for cryogenic S-parameter measurements at milli-Kelvin temperatures," *IEEE MTT-S Int. Microw. Symp. Dig.*, San Diego, CA, USA, Dec. 2023, pp. 561–564.

[14] J. Martens, "On quantifying the effects of receiver linearity on VNA calibrations," in *Proc. 70th ARFTG Microw. Meas. Conf.*, Tempe, AZ, USA, 2007, pp. 1–6.

[15] S. Krinner et al., "Engineering cryogenic setups for 100-qubit scale superconducting circuit systems," *EPJ Quantum Technol.*, vol. 6, no. 1, pp. 1–29, May 2019.

[16] J. Fitzpatrick, "Error models for systems measurement," *Microw. J.*, vol. 21, no. 5, pp. 63–66, May 1978.

[17] H.-J. Eul and B. Schiek, "A generalized theory and new calibration procedures for network analyzer self-calibration," *IEEE Trans. Microw. Theory Techn.*, vol. 39, no. 4, pp. 724–731, Apr. 1991.

[18] G. F. Engen and C. A. Hoer, "Thru-reflect-line: An improved technique for calibrating the dual six-port automatic network analyzer," *IEEE Trans. Microw. Theory Techn.*, vol. MTT-27, no. 12, pp. 987–993, Dec. 1979.

[19] A. Rumiantsev and N. Ridler, "VNA calibration," *IEEE Microw. Mag.*, vol. 9, no. 3, pp. 86–99, Jun. 2008.

[20] C. A. Hoer, "Choosing line lengths for calibrating network analyzers," *IEEE Trans. Microw. Theory Techn.*, vol. MTT-31, no. 1, pp. 76–78, Jan. 1983.

[21] N. M. Ridler, R. G. Clarke, C. Li, and M. J. Salter, "Strategies for traceable submillimeter-wave vector network analyzer," *IEEE Trans. Terahertz Sci. Technol.*, vol. 9, no. 4, pp. 392–398, Jul. 2019.

[22] R. B. Marks, "Formulations of the basic vector network analyzer error model including switch-terms," in *Proc. 50th ARFTG Conf. Dig.*, Portland, OR, USA, 1997, pp. 115–126.

[23] C. P. Eiø, S. J. Protheroe, and N. M. Ridler, "Characterising beadless air lines as reference artefacts for S-parameter measurements at RF and microwave frequencies," *Proc. Inst. Elect. Eng. Sci., Meas. Technol.*, vol. 153, no. 6, pp. 229–234, Nov. 2006.

[24] M. Horibe and N. M. Ridler, "Verifying transmission phase measurements at millimeter wavelengths using beadless air lines," in *Proc. 74th ARFTG ARFTG Microw. Meas. Conf.*, Broomfield, CO, USA, 2009, pp. 1–7.

[25] J. P. Ide, "Traceability for radio frequency coaxial line standards," NPL, India, New Delhi, Tech. Rep. DES 114, Jul. 1992.

[26] N. J. Simon, E. S. Drexler, and R. P. Reed, "NIST monograph 177: Properties of copper and copper alloys at cryogenic temperatures," Nat. Inst. Standards Technol. (NIST), Boulder, CO, USA, Tech. Rep. PB-92-172766/XAB, Feb. 1992.

[27] R. A. Matula, "Electrical resistivity of copper, gold, palladium, and silver," *J. Phys. Chem. Reference Data*, vol. 8, no. 4, pp. 1147–1298, Oct. 1979.

Sang-Hee Shin (Member, IEEE) was born in Seoul, South Korea, in 1992. He received the M.Eng. degree in aeronautical engineering and the Ph.D. degree in electrical and electronic engineering from the Imperial College London, London, U.K., in 2018 and 2022, respectively.

Since 2022, he has been with the National Physical Laboratory, Teddington, U.K., as a Higher Research Scientist with the Department of Electromagnetic and Electrochemical Technologies. His current research interests include designing and manufacturing RF and quasi-optical devices for microwave, millimeter wave, and Terahertz applications using additive manufacturing techniques, on-wafer RF measurements, and high-frequency metrology for cryogenic quantum computing applications.

Manoj Stanley (Member, IEEE) received the Ph.D. degree in electrical engineering from the University of Liverpool, Liverpool, U.K., in 2019.

He is currently a Senior Research Scientist with the Electromagnetic Technologies Group, National Physical Laboratory, Teddington, U.K. He has led and supported the development of next-generation computing and communications technologies and high-frequency electronics applications. He is developing high-frequency metrology capabilities to characterize quantum and microwave devices at cryogenic temperatures for quantum computing applications.

James Skinner (Member, IEEE) joined the National Physical Laboratory (NPL), Teddington, U.K., in November 2016. He specializes in vector network analyzer (VNA) calibration and impedance metrology and is involved in the maintenance of the primary national standards for impedance measurements and the maintenance and development of systems for traceable S-parameter measurements from kilohertz to sub-terahertz frequencies. His current research interests include metrology for sub mm-wave waveguides, cryogenic coaxial measurements, and optimization of VNA calibration techniques for coaxial and on-wafer measurements.

Sebastian E. de Graaf is currently with the National Physical Laboratory, Teddington, U.K.

Nick M. Ridler (Fellow, IEEE) received the B.Sc. degree from the King's College London, University of London, London, U.K., in 1981.

He is currently the Head of science with the Electromagnetic and Electrochemical Technologies Department, National Physical Laboratory (NPL), Teddington, U.K. He is an NPL Fellow and an Honorary Professor with the University of Glasgow, Glasgow, U.K., and the University of Liverpool, Liverpool, U.K., and a Visiting Professor with the University of Kent, Kent, U.K.; the University of Leeds, Leeds, U.K.; and the University of Strathclyde, Glasgow. He has more than 35 years' experience working in industrial, government, and academic research establishments. His current research interests include precision high-frequency electromagnetic measurement (from 1 kHz to 1 THz).

Mr. Ridler is also a Non-Executive Director of LA Techniques Ltd., a Fellow of the Institution of Engineering and Technology (IET), and a Fellow of the Institute of Physics (IOP).